2

Computational Fluid Dynamics simulations: an approach to evaluate cardiovascular dysfunction

Eduarda Silva, Senhorinha Teixeira and Pedro Lobarinhas
University of Minho
Portugal

1. Introduction

The cardiovascular system is an internal flow loop with multiple branches in which blood circulates to transport nutrient and waste throughout the body. The heart is responsible to pump blood through the cardiovascular system consisting of a complex network of three types of vessels: arteries (distribution system), capillaries (diffusion and filtration system) and veins (collection system). To accomplish their function of distribute blood through the body, the vessels are not rigid but elastic tubes that constrict or dilate (Ku, 1997; Taylor & Draney, 2004).

Blood flow in the cardiovascular system is a transient phenomenon as a result of the cyclic nature of the heart. This means that, at a given point, the velocity and pressure conditions do change with time. In fact, in the circulatory system the velocity assumes a pulsatile behavior, varying between zero, when the aortic valve is closed, and high velocities during the systole (Taylor & Draney, 2004).

Although blood flow is normally laminar, the pulsatile nature of the flow makes possible the transition to turbulence, when the artery diameter and velocities are large, like the aorta. The branches, curves and others asymmetries that are present in the vascular system also create a tri-dimensional flow characterized by asymmetries in the velocity patterns, complicated secondary motions and even flow separation from and reattachment to the wall, causing recirculation zones (Ku, 1997; Boron & Boulpaep, 2003). These hemodynamic characteristics of blood flow have long been thought to play an important role in the pathogenesis of atherosclerosis. Diseases of the cardiovascular system are manifold and afflict millions of patients worldwide including cases of: coronary artery disease, ischemic gangrene, abdominal aortic aneurysms and stroke. Many of these disfunctions are the end result of atherosclerosis, characterized by plaque accumulation within the walls of the arteries (Taylor & Humphrey, 2009). When the plaque accumulation is significant and blocks blood flow through the artery, the local restriction is known as an arterial stenosis. Stenosis induces perturbations in the blood flow and, consequently, turbulence can occur in regions where the flow is usually laminar.

Atherosclerosis can affect all arteries of the body, but there are clear evidences that there is a predisposition to be localized at branches and bends within the cardiovascular system. This

observation reinforced and led to the now widely accepted hypothesis that there is an intimate relation between the complex velocity patterns and shear stresses and the location of atherosclerosis (Taylor & Humphrey, 2009).

The application of computational techniques has become an important tool in the investigation of blood flow in arteries, distinct from experimental techniques due to the ability to simulate velocity and pressure fields in virtual models of the cardiovascular system, predict the outcomes of interventions, and improve treatment strategies (Taylor & Draney, 2004; Chen & Lu, 2004). Furthermore, when compared to experimental investigations, computational methods are often less time-consuming and costly. Computational fluid dynamic (CFD) codes and commercial packages are nowadays very robust and they can be used in a variety of field applications from a simple two-dimensional flow case to complex three-dimensional unsteady flows. Also, with the increase of hardware capability, the use of CFD is becoming even more attractive.

CFD simulations of blood flow became the cutting edge tool to investigate cardiovascular dysfunctions. While advanced imaging and diagnosis equipments available today enable the physician to view the flow through arteries, CFD studies can go much further by quantifying phenomena difficult to describe using experimental and *in vivo* techniques including wall shear stress (WSS), mass transport, and stagnation regions (Taylor & Draney, 2004; Nanduri et al., 2009). Current application of CFD simulations of blood flow is largely focused on two major research areas: blood flow in both healthy and atherosclerotic arteries. The objective of the first approach is to compute with high accuracy the various hemodynamic patterns to better understand the vascular physiology and the mechanisms that contribute to the pathogenesis of atherosclerosis (Carneiro et al., 2008b). Alternatively, the CFD techniques can be used to understand the growth of the plaque, to predict rupture risk of the plaque and test novel or patient-specific intravascular devices prior to *in vivo* implementation (Kagadis et al., 2008).

In order to compute accurately blood flow, the CFD model needs to be developed bearing in mind the special requirements of this particular application. As mentioned before, blood flow can be firstly characterised for its unsteadiness. For this reason, the computational model needs to be able to compute complex gradient of velocities that can be extremely variable along the cardiac cycle. Also, blood itself should be modelled as a two-phase non-Newtonian fluid, because it is, in fact, a suspension of a large variety of cells in plasma. Another particularity of human vascular system is the flexibility and motion of the arteries wall. Gathering all these complex characteristics in a unique CFD model is a demanding aim and, since 1970s, many groups have developed and utilized these techniques without completely achieving a full realistic model. Still, enormous progress has been done mainly due to an increase in computational capabilities and to the development of more complex and adequate numerical methods. Nowadays, each research group are oriented to understand the impact of one or two of the above characteristics but not all (Nanduri et al., 2009). In this book chapter, special insight is given to the importance of generating more accurate and realistic geometries and the demand for robust grid generation techniques. The grid generation is a major problem and often takes more person-hours to construct the grid than it does to construct and analyze the physical solution.

A tri-dimensional computational model of the abdominal aorta and renal branches is presented. The model was developed using Fluent 6.3.26 as the CFD tool and results will show the ability to predict the unsteady flow patterns throughout the cardiac cycle. The

abdominal aorta and renal branches were selected in this study for being a region where atherosclerotic disease is likely to occur (Wood, 1999). In order to solve the complex changes in the velocity gradients, induced by the pulsatile cardiac waveform, the grid has to be sufficiently dense to make possible the proper calculation of the gradients. On the other hand, the grid cannot be so dense that the solution is impractical to obtain. Therefore, different grids were developed to compare element types and grid generation strategies. For all of them, the quality of the mesh and the accuracy of the solution were studied.
One of the advantages of using computer models is the flexibility and the reduced costs in testing alternative configurations and simulation parameters. For these reasons, after developing the entire model, parallel studies were developed to infer on the simplifications validity and to study alternative parameters regarding the geometric domain.
Finally, a general overview of additional pertinent issues is given to elucidate on the different possible strategies to optimize the model. The CFD models should be held as a permanent work in progress. There are always additional phenomena that can be included and, by increasing the grade of complexity, a better understanding on the biomechanics of blood flow will be achieved.

2. Blood flow in arteries: review of computational models

The relationship between blood flow in arteries and, the sites where atherosclerosis develops, has motivated much of the research on blood flow in the past four decades (Berger & Jou, 2000). There are many branches from the aorta to the major arteries, each of them divided again in smaller arteries and so on until the capillary bed, that have been, for a long time, pointed out as initial predilection sites to manifest atherosclerosis (O'Brien & Ehrlich, 1977). A brief description of the main studies and the most relevant achievements will be presented to give an overview on the tremendous advances that have been made in this field. Firstly, special attention will be given to studies in healthy arteries, followed by CFD models to evaluate stenosed arteries.
The first attempt to model flow in normal blood vessels remotes the decade of 1950s. Womersley (1955) analyzed the equations of viscous motion for laminar flow of a Newtonian and incompressible fluid in as infinitely long and straight circular pipe. The main issue was to calculate the velocity and flow rate in arteries according to the pressure gradients measured by McDonald (1955). The physiologic pressure obtained by McDonald was represented as a Fourier series to compute the velocity profiles. The main simplifications of this study were: the assumption of a rigid circular tube to represent large arteries and the assumption of a periodic pressure gradient only function of time, whereas it is generated by a pulse wave of finite velocity. To improve these limitations, in 1957, the same author included the wall motion in his model, expressed by equations for a thin, uniform and linearly elastic wall. The Womersley analysis was useful to gain a general understanding of the relevant forces involved in arteries flow (Ku, 1997). In 1977, O'Brien and Ehrlich presented an idealized model of the trifurcation flow in renal arteries. Renal arteries are bilateral side branches that form a trifurcation branch with the abdominal aorta. The geometry was assumed as two-dimensional and straight-sided, instead of curved and three-dimensional. Despite of being a very simplified model, it showed, at that early stage, the complexity of the unsteady flow patterns at a trifurcation and the relation to the development of atherosclerosis. The comparison of steady and unsteady results

demonstrated that the WSS and recirculation were highly related and time-dependent through the cardiac cycle. The finite-difference calculations presented in this study may not be quantitatively highly accurate but they seem to present a very valid qualitative tendency of flow patterns. The limited computational resources at this stage forced this study to be two-dimensional, which may exclude certain features of the flow, such as secondary motions and circumferential variations of shear stress, features that may be critical to atherogenesis and plaque growth.

Avolio (1980) used the linear form of the Navier-Stokes equations to model wave propagation in the human arterial system. A multi-branched model of the human arterial system with 128 segments was constructed based on anatomical branching structure. The arterial segments were represented by uniform elastic tubes and characterized by electrical transmission-line properties. The work by Avolio (1980) represented significant improvements compared with previous electrical analogue models but it has been demonstrated that the complete blood flow patterns, such as secondary motion, cannot be obtained with a simpler 1D method.

Until fairly recently, the computational models used to predict blood flow were restricted to one or two dimensions. The transition to three-dimensional models, as a result of increasing computational hardware capability, had an enormous impact on the understanding of vascular hemodynamics since the problem could be described more properly than using 1D and 2D methods. Perktold & Rappitsch (1995) describe regions where separation and recirculation are expected to occur in a carotid artery bifurcation. The simulations used the time-dependent, three-dimensional, incompressible Navier-Stokes equations for non-Newtonian fluids. The complex rheological behaviour of blood was approximated using a shear model, where the apparent viscosity was expressed as a function of the shear rate. In this investigation, the effect of the distensible artery wall was also studied and it was described as a coupled fluid-structure interaction because the fluid motion and the wall motion are coupled. The velocity profiles, WSS distribution and the zones of reversed flow were obtained throughout the cardiac cycle. These results were compared with previous studies from the same authors, in which an independent ring model was used, and they shown that the coupled fluid-structure was more realistic and with influence on the flow dynamics. However, a relation between the results and atherogenesis was not established. Later, Rappitsch & Perktold (1996) proposed a numerical analysis for an axisymmetric domain in order to study the influence of the flow patterns, such as WSS and reversed flow, on the mass transport.

Steinman et al. (1996) showed good agreement between measurements of blood velocity profiles obtained by MRI (Magnetic Resonance Imaging) and numerical simulations. So far, no direct comparisons between MRI measurements and numerical simulations have been made previously and this study was important to remark the validity of numerical modelling in providing an accurate solution that can easily match MRI *in vivo* results.

The application of the finite element method to qualitatively and quantitatively assess the blood flow field in abdominal aorta was described in the investigation by Taylor et al. (1998a, 1998b). The velocity profiles were obtained under resting and exercise conditions. It was noted that under resting conditions, a recirculation zone was formed along the posterior wall of the aorta, immediately distal to the renal vessels. Low values of time-averaged WSS were present in this location and these low shear areas are hypothesized to be more susceptible to cholesterol accumulation and atherogenesis. Under moderate

exercise conditions, all regions of low WSS and high oscillatory shear index were eliminated. The investigations proved that exercise is one important mechanism increasing blood flow and WSS and it can represent a protection from atherosclerosis (Taylor et al., 2002). Following a different approach, Shipkowitz et al. (1998, 2000) and Lee & Chen (2002, 2003) developed numerical procedures based on finite volume method to simulate the flow in the abdominal aorta and its peripheral branches. Shipkowitz et al. (1998) compared the influence of assuming an axial uniform or a fully developed axial velocity profile in the inlet boundary condition and reported similar results for both. Lee & Chen (2002, 2003) demonstrated that a steady inflow may fairly describe the time-averaged blood flow behaviour when compared with a corresponding pulsatile case. Carneiro et al. (2008a) evaluated whether branches located upstream in the abdominal aorta lead to more complex flow patterns downstream.

Although numerous studies of blood flow have been conducted, only in the last decade they started to be based on realistic anatomies, acquired from computed tomography (CT) or MRI. It is well established that CFD simulations of blood flows require accurate reconstruction of geometry via imaging techniques. Cebral et al. (2002) developed a method for detail assessment of vessel anatomy and flow rate from MRI angiographic data. More recently, Kagadis et al. (2008) and Nanduri et al. (2009) presented cardiovascular models reconstructed from CT scan and they use them to conduct CFD simulations. These models can have a significant impact in medical interventions for being able to characterize non-invasively blood flow in patient-specific models.

For healthy vessels, blood flow is typically laminar but the presence of vascular diseases can generate turbulence during part of the cardiac cycle. He & Jackson (2000), in their studies on fundamental aspects of turbulence dynamics, observed that turbulence intensity is attenuated in accelerating phases and increased in decelerating phases of the cardiac cycle, mainly associated with the radial propagation of turbulence.

Turbulent flow in stenosed pipes has also been numerically studied to analyze which turbulence model could be more suitable in predicting flow profiles in stenosis region. One example of this investigation was carried out by Varghese & Frankel (2003). They simulated pulsatile turbulent flow in a rigid wall stenosed tube. The goal of their study was to predict, through direct numerical simulations, the flow features downstream of a stenosis under both steady and pulsatile conditions. The conclusions of this study indicated that the acceleration of the fluid through the stenosis resulted in WSS magnitudes that exceeded upstream levels, but WSS levels accompanied the flow separation zones that formed immediately downstream of the stenosis.

Li et al. (2007) developed a simulation model including fluid-structure interaction (FSI) and a turbulence model with realistic boundary conditions in a vessel with different degrees of stenoses. To reach this objective, the investigators performed a coupled simulation process through two commercial packages, Fluent and Abaqus, for the flow modeling and wall deforming calculation, respectively. This work shown that severe degree of stenosis causes a higher pressure drop across the vessel constriction, resulting in both higher blood velocities and peak WSS. Another relevant observation of this study pointed out the intimate correlation that exists between the increase of stenosis degree and the characteristics of the wall vessel displacement. The incorporation of wall vessel displacement mechanisms in the stenosis progression, and consequent atherosclerotic plaque rupture, brought new trends in numerical analysis in stenosed vessels.

3. Implementation of a Computational Model

The development of a computational model for a cardiovascular application involves different stages. First of all, it is essential to define the anatomic region of interest and create the computer model of the region. The computer model should be representative of the anatomic region and of the complex hemodynamic. Associated with a model there is always a set of assumptions and simplifications.
The second step is the generation of a suitable grid for the geometric domain. In third place should be the acquisition of a computational solution by solving the governing equations and the extraction of relevant hemodynamic information.

3.1 Mathematical equations

The mathematical description of pulsatile blood flow is possible by applying mass and momentum conservation. The mass of fluid is conserved, which means that the rate of increase of mass inside the element is equated to the net rate of flow of mass into the element across its faces. This relation is given by the mass conservation or continuity equation:

$$\frac{\partial \rho}{\partial t} + \rho \frac{\partial u_i}{\partial x_i} = 0 \tag{1}$$

where ρ stands for density, t for time, x_i $(i = 1, 2, 3)$ or (x, y, z) are the three-dimensional Cartesian coordinates and u_i or (u_x, u_i, u_z) are the Cartesian components of the velocity vector u.
The law of conservation of momentum (Newton's second law of motion), which states that the rate of change of momentum of a fluid particle equals the sum of the forces on a fluid particle can be written as:

$$\rho \frac{\partial u_i}{\partial t} + \rho u_j \frac{\partial u_i}{\partial x_j} = -\frac{\partial \rho}{\partial x_i} + \rho \frac{\partial}{\partial x_j} \mu \left(\frac{\partial u_i}{\partial x_j} + \frac{\partial u_j}{\partial x_i} - \frac{2}{3} \delta_{ij} \frac{\partial u_l}{\partial x_l} \right) \tag{2}$$

Where μ stands for viscosity (White, 2003).

3.2 Numerical Solution

Fluent is a general purpose computer program for modelling fluid flow and it has been used in the present implementation. It solves the conservation equations for mass and momentum using a control volume based on finite difference method. The governing equations are discretized on a curvilinear grid and Fluent uses a nonstaggered grid storage scheme to store the discrete values of dependent variables (velocities, pressure and scalars).
The first step of this method is to divide the domain into discrete control volumes. The boundaries (or faces) of control volume are positioned mid-way between adjacent nodes. Therefore, each node is surrounded by a control volume or cell. The physical boundaries should coincide with control volume boundaries (Versteeg & Malalasekera, 1995).

A portion of a grid 2D used to subdivide the domain is shown in Figure 1, where it is possible to observe the common notation used to identify each node, its neighbours and its surfaces.

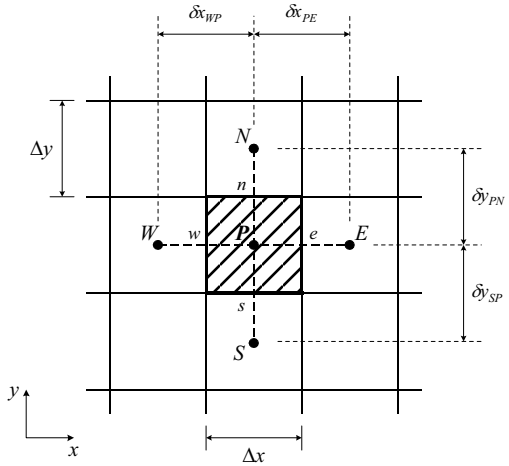

Fig. 1. A typical control volume (CV) and nomenclature used for the discretisation of equations in a 2D domain.

The integral form of the generic conservation equation for property ϕ, over a finite volume V of cross-sectional area S, is:

$$\int_{CV} \frac{\partial(\rho\phi)}{\partial t} dV + \int_{CV} div(\rho\phi v) dV = \int_{CV} div(\Gamma grad\phi) dV + \int_{CV} S_\phi dV \qquad (3)$$

Equation 3 is re-written as integrals over the entire bounding surface of the control volume by using Gauss divergence theorem:

$$\int_{CV} \frac{\partial(\rho\phi)}{\partial t} dV + \int_{A} \rho\phi v \cdot n \, dA = \int_{A} (\Gamma grad\phi) \cdot n \, dA + \int_{CV} S_\phi dV \qquad (4)$$

where vector n is the outward unit normal to surface element dA, and A is the cross-sectional area of control volume face (Versteeg & Malalasekera, 1995). Assuming that the density of fluid, velocity components and source term are known ϕ is the only unknown. The net flux through the CV boundary is the sum of integrals over the four (in 2D) or six (in 3D) CV surfaces:

$$\int_A f \, dA = \sum_j \int_{A_k} f \, dA \qquad (5)$$

where f is the component of the convective $(\rho\phi v \cdot n)$ or diffusive $(\Gamma grad\phi \cdot n)$ flux vector in the direction normal to CV surface.
The simplest approximation to the integral is the midpoint rule. The integral is approximated as a product of the integrand at the cell-face centre (which is itself an approximation to the mean value over the surface) and the cell-face area (Ferziger & Peric, 2002):

$$F_e = \int_{A_e} f \, dA = \bar{f}_e A_e \approx f_e A_e \tag{6}$$

Since the value of f is not available at the cell face centre *e*, it has to be obtained by interpolation of nodal values of the solution. This interpolation must have at least the same order of accuracy as that of the integration scheme. In order to preserve the second-order accuracy of the midpoint rule approximation of the surface integral, the value of f_e has to be computed with at least second-order accuracy.
For the temporal discretization of the first term in the conservation equations, the implicit Euler scheme has been used.
The integration of the differential equations in each control volume yields a finite-difference equation that conserves each quantity (velocities, pressure and scalars) on a control-volume basis. The integral conservation equation applies to each CV, as well as to the solution domain as a whole. This basic characteristic makes the finite volume method suitable for this type of application.
The discretized equations are solved sequentially and the SIMPLE algorithm has always been used in the present application. This type of algorithm is based on using a relationship between velocity and pressure corrections in order to recast the continuity equation in terms of a pressure correction calculation. In this way, the calculated velocity and pressure fields satisfy the linearized momentum and continuity equations at any point.
The system of algebraic equations for each variable is solved using a Line Gauss-Seidel procedure (LGS). To speed up the convergence achieved by the LGS procedure, Fluent uses a Multigrid acceleration technique by default to solve the pressure equation.
Fluent does not solve each equation at all points simultaneously and so an iterative solution procedure is used with iterations continuing until the convergence criteria specified has been achieved.
The new calculated values of a given variable obtained, in each iteration by the approximate solution of the finite difference equations are then updated with the previews values of the variable using an underrelaxation technique. The user can choose the best relaxation factors for each variable in order to achieve a better convergence.

3.3 Boundary Conditions

Numerical simulations were carried out assuming a Newtonian and incompressible behaviour on the fluid. The fluid was set as water-liquid but the viscosity was assumed as 0.0035 kg/ms and density 1056 kg/m^3, which are the properties of blood.
Simulations in this study were run for a pulse cycle raging from velocities close to zero, during the diastole, to a maximum velocity of 0.35 m/s, during peak systole, according to a representative suprarenal blood flow waveform calculated by Taylor & Draney (2004).

Using a representative and common abdominal aorta diameter (D=0.022 m) and considering the assumed fluid properties (viscosity and density), the mean Reynolds number is Re=730. For this reason, the flow was firstly modelled as laminar.

3.4 Geometry and Grid

In order to capture accurate local fluid dynamics in the abdominal aorta and renal branches, the geometry must be representative of the native anatomy. In this study, the geometry was constructed based on two different models proposed by Shipkowitz et al. (1998) and Lee & Chen (2003), both of them deduced from statistical data. The complete geometric domain of the idealized abdominal aorta model is presented in Figure 2.

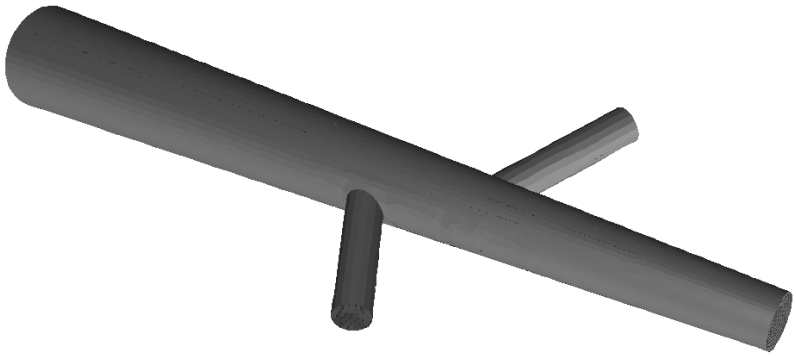

Fig. 2. Illustration of the abdominal aorta model with the renal arteries.

In the present computational model, the major simplifications are associated with the assumption of rigid and straight arteries, which neglects the walls motion and curvature. Also, blood was considered as a Newtonian fluid.

In a finite volume approach it is necessary to discretize the domain using a grid (mesh). The accuracy of the CFD solution is governed by the number of cells and choice of which element type to use in the grid. In a previous study, four different grids were developed in order to compare the performance of different element type and mesh generation strategies (Fig. 3) (Silva et al., 2008). It is relevant to establish a relation between grids and accuracy in the results obtained in Fluent simulations.

It is relevant to point out that the grid has a noticeable effect on CFD results and for this reason the automatic grids (tetrahedral) are usually not adequate and they may compromise the validity of results.

4. Grid Optimization

Generating a grid requires a good understanding about element types, the appropriate distribution of elements over the domain, the strategy to use in the decomposition of the domain and the necessity of boundary layers. In this study, four different grids were obtained, using Gambit, in order to compare the performance of different element types and mesh generation strategies.

Regarding the element type, the first approach was the tetrahedral grid because tetrahedral elements can easily adapt to complicated geometries and, for this reason, the grid can be

obtained quick and automatically (Grid (1)). However, the homogeneous distribution of the elements did not seem adequate because it is essential to have high dense grid in the bifurcation regions where the flow becomes more complex. Actually, an optimal grid is often non-uniform: denser in areas where large variations occur from point to point and coarser in regions relatively stable. Consequently, in a new grid, a combination of tetrahedral and hexahedral elements was used. This allows high grid quality to be achieved throughout the domain and an appropriate distribution of each element type – hybrid grid (Grid (2)). Although the element distribution was improved, still all bad quality elements were located in the tetrahedral grid. For this reason, special efforts were made in order to divide the domain in different volumes. In each of them it was possible to generate hexahedral grids (Grid (3)).
In this study, as atherosclerosis lesions are expected to be located along the walls, it is important to characterize the flow patterns near the walls. In this way, boundary layers were implemented along the walls in order to capture the fluctuations in the flow field caused by the bifurcations. Since there is one plane of symmetry, the geometry can be divided in two equivalent parts which reduces significantly the computational time (Grid (4)).

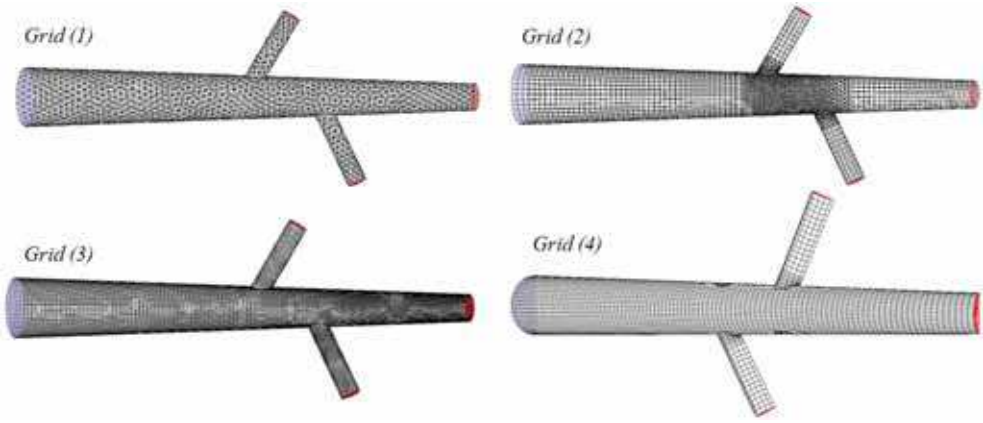

Fig. 3. Overview of the four different grids generated.

4.1 Grid Quality

Skewness is usually considered a parameter to evaluate mesh distortion and it has a significant impact on the accuracy of the numerical solution. Highly skewed cells can decrease accuracy and destabilize the solution.
Figure 4 illustrates what skewness represents for a 2D face. It is the angle between the area vector and the vector connecting the two cell centroids. An angle of zero indicates a perfectly orthogonal mesh which means that optimal quadrilateral meshes will have vertex angles close to 90 degrees, while triangular meshes should preferably have angles of close to 60 degrees and have all angles less than 90 degrees (CD-adapco STAR-CCM+, 2000-2006).

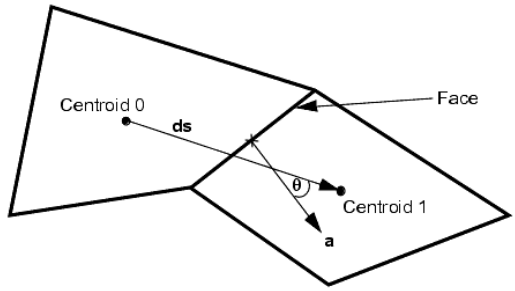

Fig. 4. Illustration of the skewness for a two-dimensional face (Adapted from CD-adapco STAR-CCM+, 2000-2006).

The quality of each grid was studied according to properties of skewness. In order to do this, two skewness measures were calculated, EquiAngle Skew and EquiSize Skew. For both properties, smaller values are more desirable (Table 1). In quantifying the quality of each grid, values of EquiAngle Skew and EquiSize Skew of 0–0.25 are considered excellent, 0.25–0.5 are good and 0.5–0.75 are fair. Grid (1) shows very high quality and the elements seem to adapt very well to the geometry. However, as explained before, the distribution of elements over the domain is not satisfactory. Furthermore, the use of hexahedral elements reduces the number of cells and, consequently, the CPU time. Grid (2) represents a good progress in terms of distribution, but the quality was reduced. A closer look on the bad elements (outside the interval 0-0.75) shows that all of them were located in the tetrahedral grid. Grid (3) is an entirely hexahedral grid. The implementation of this grid involves the partition of the domain in 8 volumes. The objective is to split the model into areas that can be meshed separately, while creating a uniform combination and allowing the lowest value of skewness possible. However, as smaller and more intricate volumes are created, the resulting elements tend to be smaller. Consequently, the quality is compromised, especially near the walls. This is the reason why the quality of Grid (3) is reduced. The same happens in Grid (4), due to the boundary layers implementation (which means a concentration of small elements near the walls). However, in order to evaluate grids, not only skewness properties should be compared, but also the accuracy of the computational solution.

Grid (1)	
EquiAngle Skew (0-0.75)	99.97%
EquiSize Skew (0-0.75)	100%
Grid (2)	
EquiAngle Skew (0-0.75)	99.95%
EquiSize Skew (0-0.75)	99.98%
Grid (3)	
EquiAngle Skew (0-0.75)	99.93%
EquiSize Skew (0-0.75)	99.93%
Grid (4)	
EquiAngle Skew (0-0.75)	99.83%
EquiSize Skew (0-0.75)	99.83%

Table 1. Grid quality evaluation for the four grids based on parameters of skewness.

4.2 Grid Accuracy

So far, the comparison between grids was made in terms of element type used, strategies of grid refinement and parameters of quality. However, it is also important to establish a relation between grids and the accuracy obtained in CFD simulations. A steady simulation was defined with a constant inlet velocity of 0.35 m/s, representing the maximum velocity of pulsatile profile.

Figure 5 shows the axial velocity contours in the axial plane 90 mm downstream the inlet boundary. This cross-section divides the abdominal aorta and the left renal branch. It is important that the grid imposes a smooth transition between the velocities near the walls, at abdominal aorta and renal artery, and the central flow. Grid (1), Grid (2) and Grid (3) show a very asymmetric and non-uniform distribution of axial velocities, principally in the renal wall. The external contour of the cross-section in Grid (1) proves that the tetrahedral elements cannot represent properly the circular geometry.

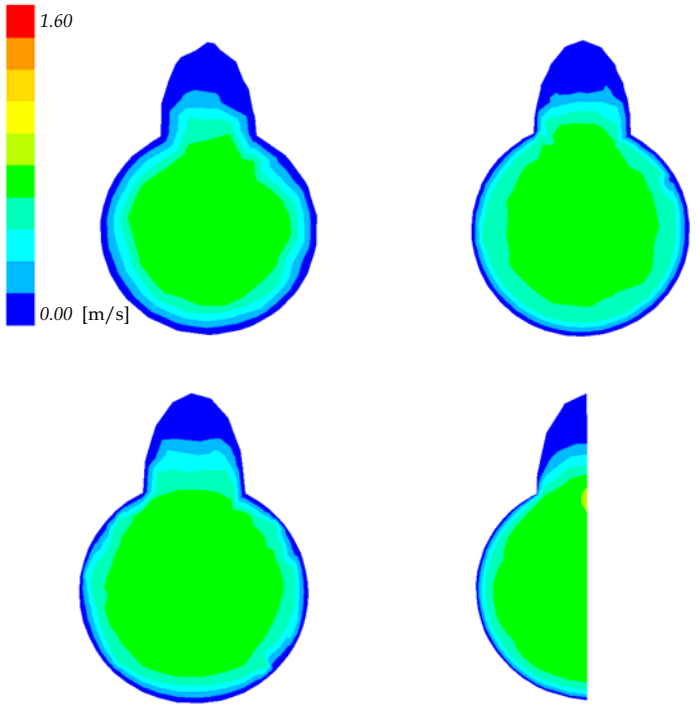

Fig. 5. Axial velocity contours at the axial plane 90 mm downstream the inlet boundary.

The implementation of boundary layers in Grid (4) shows a good effect in terms of a smooth transition from zero to maximum velocities and also improves the symmetry (this was proved for an equivalent grid in which the symmetry assumption was neglected). For being a good quality grid, with good parameters of symmetry and acceptable number of cells, Grid (4) was selected after the grid generation process.

4.3 Grid Density

To demonstrate the quality of the computational solution, it is essential to prove that the CFD results are grid independent. In other words, the results in terms of flow distribution are not dependent on the grid and they are only a consequence of the simulation parameters. Once the optimal grid generation strategy is achieved, different grids with different densities should be generated. The purpose is to evaluate if the solution converges to a value when the number of elements tends to infinite, which demonstrates that the results are independent on the grid, although the accuracy increases with the number of cells. Although accuracy increases with finer grids, the CPU and memory requirements to compute the solution and postprocessing also increase. Equilibrium must be established between the solution accuracy and computational time. In order to overcome the computational limitations, a variety of parallel paradigms have been implemented to parallelize the CFD codes and consequently speedup the computational jobs compared to the speed of a single computer.

5. Results

5.1 Velocity Profiles along the cardiac cycle

The axial velocity profiles, secondary motion and recirculation in abdominal aorta and renal branches were obtained and results are showed in Figure 6. The four different times illustrate the different phases of the cardiac cycle: acceleration phase (0.13 s), peak systole (0.25 s), deceleration phase (0.4 s) and diastole (0.8 s).

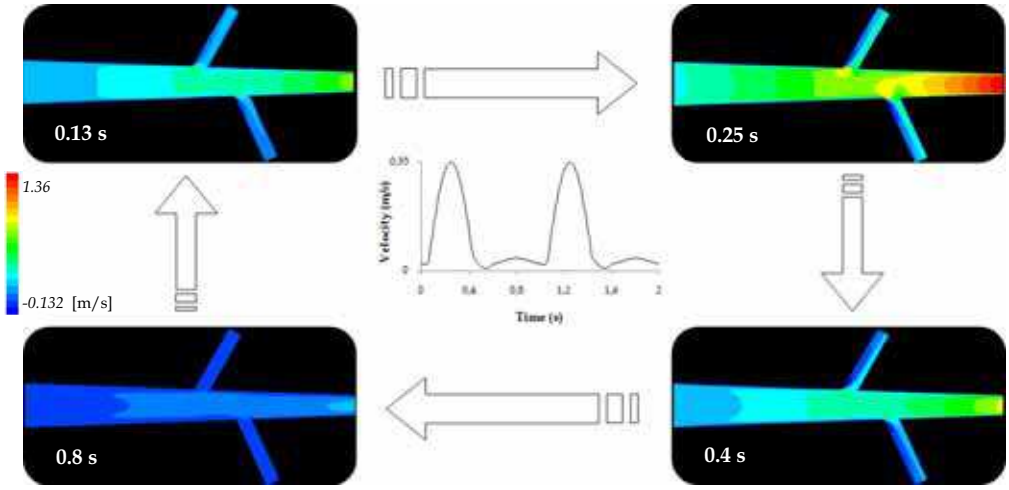

Fig. 6. Axial flow velocity profiles at the mid-frontal plane at 0.13 s, 0.25 s, 0.4 s, 0.8 s.

Comparing the velocity profiles, it can be concluded that the flow patterns are highly different along the cardiac cycle. The flow in the two renal arteries is also slightly different since they are not symmetric and geometrically the branching angles are different as well.
Flow results at renal branches proved the occurrence of flow separation since flow divides into two streams: maximum velocity at the distal wall of the bifurcations and slower moving fluid on the proximal wall (Fig. 7). Also, flow separation is more noticeable in the peak

systole and deceleration phases and it drops at the diastole phase. These blood flow patterns may be related to the development of atherosclerosis plaque at this location.
The present characterization of velocity fields, under laminar conditions, enables the comprehension of the abdominal aorta and renal arteries hemodynamics.

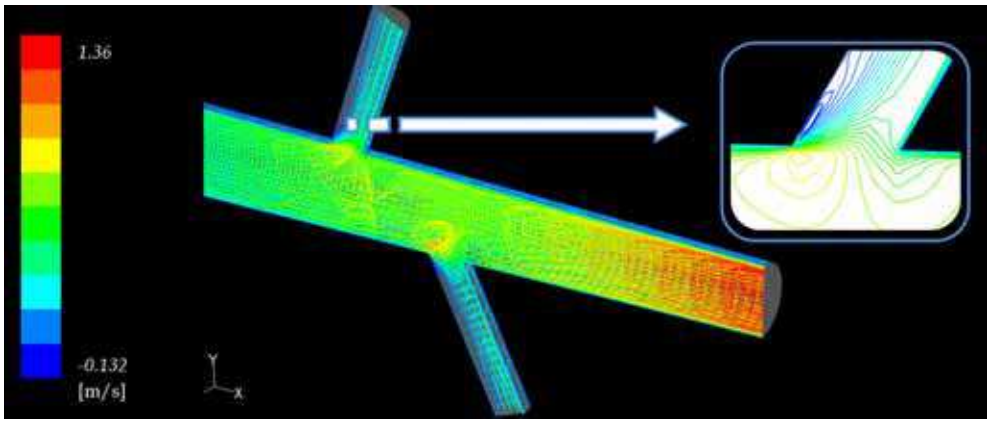

Fig. 7. Detail on the recirculation region at peak systole.

5.2 Shear-Stress analysis at wall boundaries

As blood flows across the endothelium, WSS is generated to retard the flow. Therefore the WSS (τ) represents the force acting tangential to the surface due to friction.
In laminar flows the WSS only depends on the velocity gradient at the wall, and the fluid dynamic viscosity. For no-slip wall conditions, generally applied in these studies, the properties of the flow adjacent to the wall/fluid boundary are used to predict the shear stress on the fluid at the wall. In a laminar flow, the WSS is therefore defined by the normal velocity gradient at the wall as (Fluent 6.2, 2005):

$$\tau = \mu \frac{\partial v}{\partial n} \tag{7}$$

Since the blood flow is highly skewed, the distribution of the WSS must be measured along the cardiac cycle by detailed velocity profiles very close to the wall (Wootton & Ku, 1999).
The distribution of WSS through a line along the abdominal aorta, proximal and distal renal walls is illustrated in Figure 8. The results show that WSS in the abdominal aorta wall tends to increase along its length and especially in the neighborhood of the renal branch. At the renal walls, the WSS distribution along the proximal wall deviates significantly from that found along the distal wall: low WSS at the proximal wall and high WSS at the distal renal wall.
The appearance of this low WSS in the proximal wall coincides with the presence of recirculation. Along the distal wall the WSS reaches a maximum in the entry of the bifurcation and tends to decrease along the distance.

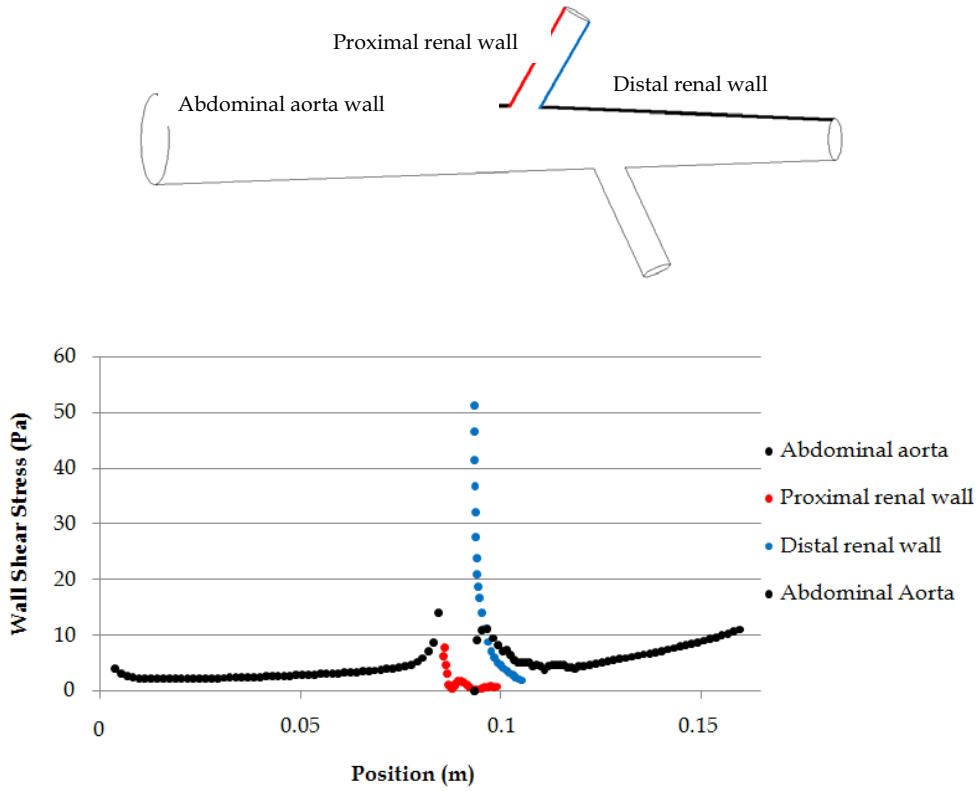

Fig. 8. WSS along abdominal aorta, proximal and distal renal arteries.

5.3 Fully developed inlet velocity

Two different configurations on the inlet velocity boundary condition were studied, either a uniform velocity or a fully developed velocity profile, both of them based on a physiologic velocity profile at peak systole.

Considering that, for laminar flow, the velocity inside a tube varies according to the equation:

$$u = \frac{\Delta p}{4\mu}\left(R^2 - r^2\right) \tag{8}$$

From Equation 8, the maximum velocity corresponds to r=0 and it can be written like:

$$u_{\max} = \frac{\Delta p R^2}{4\mu} \tag{9}$$

Assuming that the maximum velocity is twice the average velocity and combining this relation with Equation 9, results:

$$u = \frac{u_{\max}}{R^2}\left(R^2 - r^2\right) \tag{10}$$

Equation 10 can be written for rectangular coordinates, instead of cylindrical coordinates, in which yz coordinates correspond to the nodes coordinates in the inlet face (White, 2003):

$$u = u_{\max}\left(1 - \left(\sqrt{\frac{y^2 + z^2}{R}}\right)\right)^2 \tag{11}$$

In the uniform velocity configuration the velocity was set to 0.35 m/s, while in the fully developed flow the velocity varies along the inlet face according to equation 11 and assuming that u_{max} is 0.7 m/s.

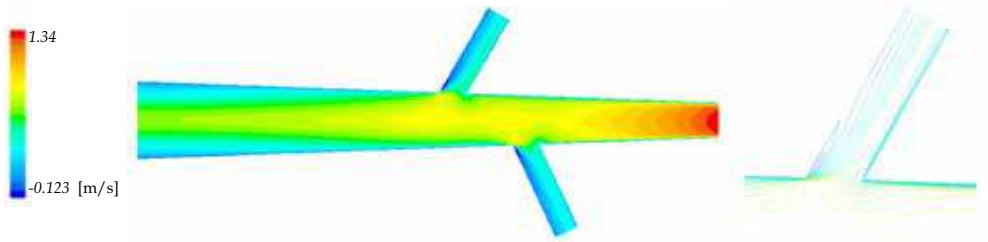

Fig. 9. Axial velocity profiles and iso-velocity lines at the mid-frontal plane for uniform (a) and fully developed (b) inflows.

The velocity contours show similar velocity distributions for both uniform and fully developed boundary condition (Fig. 9). The highest and lowest velocities are in the same range and they are found in the same locations. However, as expected, different flow patterns are obtained, specially, in the upstream portion before the bifurcations. Futhermore, the recirculation length is approximately the same in both cases. It seems that, apparently, the change in the inlet velocity does not affect the fluid dynamics in the complex regions.

5.4 Computational model based on *in vivo* anatomic images

The previous characterization of velocity fields and WSS distributions, under laminar condition, enables the comprehension of the abdominal aorta and renal arteries hemodynamics in idealized models. Afterwards, some investigations were made in order to infer about the sensibility of the model to the geometric domain. The impact of using *in vivo* anatomic images (obtained by CT) was analysed.

The computational method described herein was used to develop a model of the abdominal aorta and renal branches obtained from CT images of a normal adult subject. Our purpose is to compare the computational results obtained from a realistic and an idealized anatomic geometry.

CT scans the body and produces an image of each slice. The information from CT scan can be saved in a standard digital format called DICOM (Digital Imaging and Communications in Medicine). This is a universal file type, developed to facilitate data exchange between hardware, independently of manufacturer (Graham et al., 2005). The 2D images produce by CT systems can be assembled to produce complete 3D representations of scanned components with 3D image segmentation and volume rendering software. In the current project Mimics was used to produce the 3D model. To obtain a 3D model from 2D CT images, some steps were followed:

- After loading the CT images in Mimics, the first step was to segment the images, by applying filters of gray values, in order to select only the specific tissues of interest. In this case, the pixel range used to select the arteries is also the pixel range for other tissues (Fig. 10) For this reason the dynamic region growing tool was used to segment the CT images based on the connectivity of gray values in a certain pixel range.
- The final 3D object was constructed based on the previous image segmentation. This volume was exported as STL file to a Computing Aided Design (CAD) software, such as SolidWorks.
- The 3D model obtained directly from rendering the CT images had too much interference in its surface, which disable the appropriate mesh generation. Consequently, a second model was constructed in SolidWorks, using the first model as source for dimensions, curvature and bifurcation axes.
- The model obtained was then exported to Gambit as an ACIS file (version 10.0) and it was automatically meshed with tetrahedral elements.

The results presented here are very preliminary and comparisons can only be performed in a rough qualitative manner. Velocity contours are shown in Figure 11. The flow fields are highly different in terms of magnitude and patterns: the maximum velocity is no longer found in the outlet face but in the neighborhood of the right artery. Also, the abdominal aorta curvature seems to have a decisive impact in the flow fields.

The differences found between these two models do not compromise the validity of the previous results, mainly, because the procedure of 3D model generation from CT images needs to be improved and more carefully understood. On the other hand, the comparison between these two models should be seen as a suggestion to the importance of using *in vivo* data.

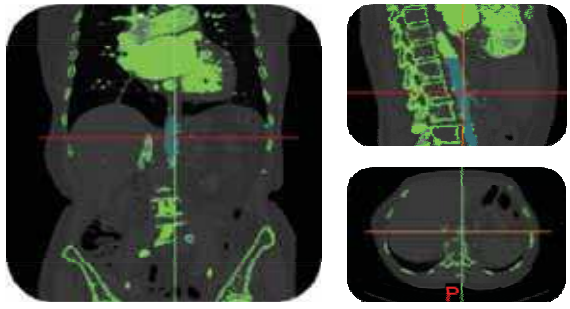

Fig. 10. Two-dimensional CT images and the result of the image segmentation.

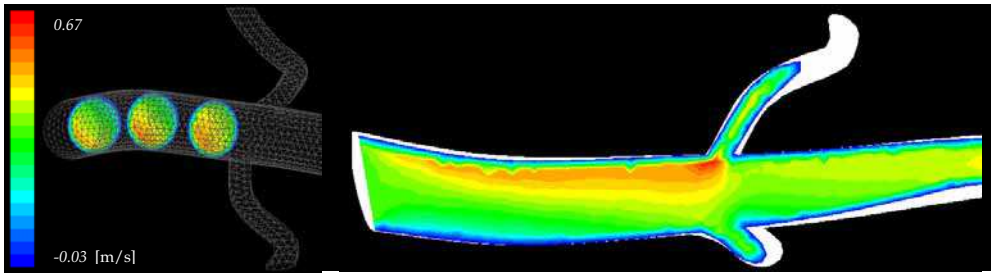

Fig. 11. Velocity profiles for the model obtained from CT images

6. Model Optimization

A model is, by definition, an approximation to reality. There are several reasons that contribute for this outcome; one of the most important is limitation in computational capacities. The closer the model gets to the real behaviour of the structure it is trying to emulate, the more complex it gets. Therefore there is, currently, no model that perfectly mimics the blood flow and blood vessels performance. Instead, there are different models that better contribute to the understanding of different phenomena. This topic on model optimization attempts to give an insight on the different paths that can be followed to increase the accuracy (and, inevitably, the complexity) of a model of cardiovascular structures. It is important to understand that when a research aims to give a deeper knowledge on a phenomenon through the application of computational models it is, most commonly, obliged to neglect some aspects. This is why this topic is crucial. It portraits the approaches that are made depending on the goal of the research. Each of the following points represents one of the parameters for which CFD has been perfected, thus contributing to the progress of the state-of-the-art.

6.1 Compliance of arterial walls

Various computational models, with rigid or compliant tubes, have been used to quantify flow and wall mechanical behaviors. It has been found that artery stiffness, stenosis geometry are the dominating factors affecting blood flow and artery motion.

FSI is a relatively new technique used in numerical problems to provide a better understanding on the blood flow characteristics because it includes the flow impact on structures (mainly artery walls) and on the local hemodynamics features. However, modeling the human circulatory system remains a very difficult process because of its geometrical complexity. Consequently, a large number of special assumptions have to be considered to simulate blood flow accurately. Since, a high majority of the studies represent trunked regions of arterial tree, it is necessary to take into consideration the link between local and global blood flow phenomena. As a result, to perform more realistic numerical simulations, the challenge in the geometric modeling approaches consists in the setting of proper coupling conditions to obtain quantities such as the flow rate, and the pressure at the interfaces between different model structures.

Chakravaty & Mandal (2000) have performed important studies on blood flow in a deformable stenotic artery and their aim was to validate a method of coupling wall deformations with fluid flow. Mandal (2005) simulated similar conditions while setting the

fluid to have a different model for the fluid viscosity (Generalised Power Law non-Newtonian model). The methods employed by Mandal provided excellent results with look upon to fluid characteristics, like, fluid velocity, WSS and pressure gradients with respect to changes in stenosis shape and degree of narrow. However, their method could not provide the stress distributions across the wall as this was set to deform governing set of equations, rather than actually creating a wall model itself. Li & Kleinstreuer (2005) modeled blood flow with FSI in a stent, which then expanded within an aneurysm sac. The blood was set to have non-Newtonian properties. This work presented a three-dimensional view of the critical stresses within the stent and aneurysm as well as potential risks resulting from different flow pressures. Within our group, the effect of the artery wall deformation upon the flow patterns is also being investigated. The prime goal of this study is the development of numerical models able to predict the blood flow in the region of abdominal aorta under deformable boundaries. The simulations are being performed using adaptative dynamic meshes into Fluent (Ferreira et al., 2009).

6.2 Multiphase

Most CFD models are developed considering blood as a single-phase fluid and, as seen before, these models can accurately predict the flow patterns in three-dimensional models. Although blood behaves as a non-Newtonian fluid under certain conditions due to the rheological properties of a red blood cell-plasma suspension, it was shown that the Newtonian assumption is reasonable (Shipkowitz et al., 1998) for large arteries studies. Even though, it would be relevant to evaluate the spatial and temporal distributions of red blood cells and identify regions where adhesion and deposition to the artery walls occur. Several studies had already introduced multiphase models to study blood flow.

Following this multiphase characteristic of blood flow, some studies have presented results for a CFD models consisting of a continuous plasma phase and a dispersed RBC phase (Huang et al., 2009; Jung et al., 2009). In terms of numerical methods, Navier-Stokes equations are solved with the particular increment of a volume fraction for each phase, as well as mechanisms for the exchange of mass, momentum, and energy between the phases. Although the multiphase blood flow models proved to be in close agreement with the single-phase models, new insights were obtained about the flow characteristics that promote the migration of the cells to the arterial walls.

6.3 Microscale CFD models

The numerical simulations presented herein provide relevant information on the three-dimensional velocity profiles and they show the complex hemodynamics of blood flow in arteries. These numerical flow fields can be used to identify critical flow regions and, therefore, can be used as a powerful tool to optimize the medical devices design. However, these macroscale flow patterns do not fully describe the implications of the complex flow field to the blood cells. It is important to predict and avoid the occurrence of mechanical damage and/or destruction of platelets and red blood cells due to cardiovascular diseases or the implantation of medical devices. For these reasons, several studies are currently focused in investigating the mechanical loading on blood cells due to microscale flow structures. Liu et al., (2006) are focusing their research efforts in modeling blood flow at a cellular scale. Recently they proposed numerical methods able to compute red blood cells deformation

and aggregation, cell-cell interactions and even cell migration. Quinlan and Dooley (2007) proposed a model able to compute flow-induced stress on a single red blood cell due to turbulent blood flow. This information can ultimately be useful for blood damage prediction in the design of medical devices.

7. Conclusion

The blood flow patterns presented so far were obtained with a very good quality grid, which was developed after sequence refinements and according to the computational facilities available. It is not expected that further refinements in the mesh will result in substantial differences in the solution.

The velocity profiles reveal the presence of reversed flow throughout the cardiac cycle, especially at deceleration period. The recirculation was found at the proximal wall of the renal branches and along the posterior wall of the abdominal aorta. It has been shown that the presence of recirculation in the renal arteries is coincident with the location of low WSS. These blood flow patterns may be related to the localization and development of atherosclerosis plaque at this location. More studies need to be performed in order to establish a direct correlation between these regions and the location of vascular diseases. Even though, some studies have indicated that low WSS usually occur in regions of high probability of plaque localization (Taylor et al., 1998b). The plots of velocity patterns and WSS distribution obtained in the present work are in good agreement with previous computational and *in vivo* studies (Taylor et al., 1998b; Lee & Chen, 2002).

In this study, the inlet velocity was assumed as uniform pulsatile according to a suprarenal velocity profile obtained by Taylor & Draney, 2004. However, it is possible that velocity profiles become fully developed by the time they reach the abdominal aorta. For this reason, the two configurations were tested and the results were similar for both constant and fully developed inflow.

8. References

Avolio, A. (1980). Multi-branched model of the human arterial system. *Med & Biol. Eng. & Comput*, Vol. 18, 709-718

Berger, S. & Jou, L. (2000). Flows in Stenotic vessels. *Annu. Rev. Fluid Mech.*, Vol. 32, 347-382

Boron, W. & Boulpaep, E. (2003). *Medical Physiology,* W. B. Saunders Company, 9781416023289, Philadelphia

Carneiro, F.; Silva, A.; Teixeira, S.; Teixeira, J.; Lobarinhas, P. & Ribeiro, V. (2008a). The Influence of Renal Branches on the Iliac Arteries Blood Flow, *Proceedings of the ASME 3rd Frontiers in Biomedical Devices*, 0791838234, Irvine, California, June 2008

Carneiro, F.; Ribeiro, V.; Teixeira, S. & Teixeira, J. (2008b) Numerical study of blood fluid analogous in the abdominal aorta bifurcation, *Proceedings of 4th International Conference on Comparing Design in Nature with Science and Engineering*, 97818456412072426, Algarve, June 2008, WIT Press, Southampton

CD-adapco STAR-CCM+, 2000-2006

Chakravarty, S. & Mandal, P. (2000). Two-dimensional blood flow through tapered arteries under stenotic conditions. *Intern. J. Non-Linear Mech.*, Vol. 35, 779-793

Cebral, J.; Yim, P.; Lohner, R.; Soto, O. & Choyoke, P. (2002). Blood flow modeling in carotid arteries with computational fluid dynamics and MR imaging. *Acad. Radiol.* Vol. 9, 1286-1299

Chen, J. & Lu, X. (2004). Numerical investigation of the non-Newtonian blood flow in a bifurcation model with a non-planar branch. *Journal of Biomechanics*, Vol. 37, 1899-1911

Ferreira, A.; Teixeira, S.; Teixeira, J. (2009). Contributions to the study of blood flow in the abdominal aorta and its branches. *ASME International Mechanical Engineering Congress & Exposition*, Lake Buena Vista, Florida, November 2009

Ferziger, J. & Peric, M. (2002). *Computational Methods for Fluid Dynamics*, Springer, Berlin, Germany.

Fluent 6.2 User's Guide, (2005). Fluent Inc.

Graham, R.; Perriss, R. & Scarsbrook, A. (2005). DICOM demystified: A review of digital file formats and their use in radiological practice. *Clinical Radiology*, Vol. 60, 1133-1140

He, S. & Jackson, J. (2000), A study of turbulence under conditions of transient flow in a pipe. *J. Fluid Mech.,* Vol. 408, 1–38

Huang, J.; Lyczkowski, R. & Gidaspow, D. (2009). Pulsatile flow in a coronary artery using multiphase kinetic theory. *Journal of Biomechanics,* Vol. 42, 743–754

Jung, J.; Lyczkowski, R.; Panchal, C. & Hassanein, A. (2009). Multiphase hemodynamic simulation of pulsatile flow in a coronary artery. *Journal of Biomechanics*, Vol. 39, 2064–2073

Kagadis, G.; Skouras, E.; Bourantas, G.; Paraskeva, C.; Katsanos, K.; Karnabatidis, D. & Nikiforidis, G. (2008). Computational representation and hemodynamic characterization of *in vivo* acquired severe stenotic renal artery geometries using turbulence modeling. *Medical Engineering & Physics*, Vol. 30, 647–660

Ku, D. (1997). Blood flow in arteries. *Annu. Rev. Fluid Mech*, Vol. 29, 399–434

Lee, D. & Chen, J. (2002). Numerical simulation of steady flow flieds in amodel of abdominal aorta with its peripheral bramches. *Journal of Biomechanics*, Vol. 35, 1115-1122

Lee, D. & Chen, J. (2003). Pulsatile flow fields in a model of abdominal aorta with its peripheral branches. *Biomedical Engineering Applications, Basis & Communications,* Vol. 33, 1305-1312

Li, Z. & Kleinstreuer, C. (2005), Blood flow and structure interactions in a stented abdominal aortic aneurysm model, *Medical Engineering & Physics*, Vol.27, 369-382

Li, M.; Beech-Brandt, J.; John, L.; Hoskins, P. & Easson, W. (2007). Numerical analysis of pulsatile blood flow and vessel wall mechanisms in different degrees of stenoses. *Journal of Biomechanics*, Vol. 40, 3715-3724

Liu, W.; Liu, Y.; Farrell, D.; Zhang, L.; Wang, X.; Fukui, Y.; Patankar, N.; Zhang, Y.; Bajaj, C.; Lee, J.; Hong, J.; Chen, X. & Hsu, H. (2006). Immersed finite element method and its applications to biological systems, *Comput. Methods Appl. Mech. Engrg.*, Vol. 195, 1722–1749

Mandal, P. (2005), An unsteady analysis of non-Newtonian blood flow through tapered arteries with a stenosis, *International Journal of Non-Linear Mechanics*, Vol. 40, 151-164

Nanduri, J.; Pino-Romainville, F. & Celik, I. (2009). CFD mesh generation for biological flows: Geometry reconstruction using diagnostic images. *Computers & Fluids,* Vol. 38, 1026-1032

O'Brien, V. & Ehrlich, L. (1977). Simulation of unsteady flow at renal branches. *Journal of Biomechanics*, Vol. 10, 623-631

Perktold, K. & Rappitsch, G. (1995). Computer simulation of local blood flow and vessel mechanics in a compliant carotid artery bifurcation model. *Journal of Biomechanics*, Vol. 28, 845-856

Quinlan N. & Dooley P.(2007). Models of Flow-Induced Loading on Blood Cells in Laminar and Turbulent Flow, with Application to Cardiovascular Device Flow. *Annals of Biomedical Engineering*, Vol. 35, 1347–1356

Rappitsch, G. & Perktold, K. (1996). Computer simulation of convective diffusion process in large arteries. *Journal of Biomechanics*, Vol. 29, 207-215

Shipkowitz, T.; Rodgers, V.; Frazin, L. & Chandran, K. (1998). Numerical study on the effect of steady axial flow development in the human aorta on local shear stresses in abdominal aortic branches. *Journal of Biomechanics*, Vol. 31, 995-1007

Shipkowitz, T.; Rodgers, V.; Frazin, L. & Chandran, K. (2000). Numerical study on the effect of secondary flow in the human aorta on local shear stresses in abdominal aortic branches. *Journal of Biomechanics*, Vol. 33, 717-728

Silva, A.; Teixeira, S. & Lobarinhas, P. (2008). The influence of different grid approaches on a cardiovascular computational model, *Proceeding of the 17th IASTED International Conference on Applied Simulation and Modelling 2008*, 9780889867482, Corfu, Greece, June 2008, ACTA Press, Calgary

Steinman, D.; Frayne, R.; Zhang, X.; Rutt, B. & Ethier, C. (1996). MR measurement and numerical simulation of steady flow in an end-to-side anastomosis model. *Journal of Biomechanics*, Vol. 29, 537-542

Taylor, C.; Hughes, T. & Zarins, C. (1998a). Finite element modeling of blood flow in arteries. *Comput. Methods Appl. Mech. Engrg.*, Vol. 158, 155-196

Taylor, C.; Hughes, T. & Zarins, C. (1998b). Finite element modeling of three-dimensional pulsatile flow in the abdominal aorta: relevance to atherosclerosis. *Annals of Biomedical Engineering*, Vol. 26, 975-987

Taylor, C.; Cheng, C.; Espinosa, L.; Tang, B.; Parker, D. & Herfkens, R. (2002). *In vivo* Quantification of Blood Flow and Wall Shear Stress in the Human Abdominal Aorta during Lower Limb Exercise. *Annals of Biomedical Engineering*, Vol. 30, 402-408

Taylor, C.; Draney, M. (2004). Experimental and computational methods in cardiovascular fluid mechanics. *Annu. Rev. Fluid Mech.*, Vol. 36, 197–231

Taylor, C.; Humphrey, J. (2009). Open problems in computational vascular biomechanics: Hemodynamics and arterial wall mechanics. *Comput. Methods Appl. Mech. Engrg.,* In Press, Corrected Proof, Available online 15 February

Varghese, S. & Frankel, S. (2003). Numerical Modeling of pulsatile turbulent flow in stenotic vessels. *Journal of biomechanical engineering*, Vol. 125, 445-460

Versteeg, H. & Malalasekera, W. (1995). *An introduction to computational fluid dynamic. The finite volume method.* Longman Scientific & Technical, 9780131274983 Harlow, UK

White, F. (2003). *Fluid Mechanics*. McGraw-Hill, 9780072831801, New York

Wood, N. (1999). Aspects of fluid dynamics applied to the large arteries. *J. Theor. Biol.*, Vol. 199, 137-161

Wotton, D.; Ku, D. (1999). Fluid Mechanics of Vascular Systems, Diseases, and Thrombosis. *Annu. Rev. Biomed. Eng.*, Vol. 01, 299-329

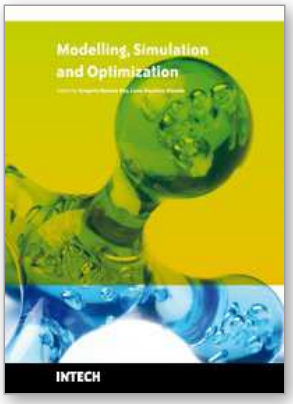

Modelling Simulation and Optimization

Edited by Gregorio Romero Rey and Luisa Martinez Muneta

ISBN 978-953-307-048-3
Hard cover, 708 pages
Publisher InTech
Published online 01, February, 2010
Published in print edition February, 2010

Computer-Aided Design and system analysis aim to find mathematical models that allow emulating the behaviour of components and facilities. The high competitiveness in industry, the little time available for product development and the high cost in terms of time and money of producing the initial prototypes means that the computer-aided design and analysis of products are taking on major importance. On the other hand, in most areas of engineering the components of a system are interconnected and belong to different domains of physics (mechanics, electrics, hydraulics, thermal...). When developing a complete multidisciplinary system, it needs to integrate a design procedure to ensure that it will be successfully achieved. Engineering systems require an analysis of their dynamic behaviour (evolution over time or path of their different variables). The purpose of modelling and simulating dynamic systems is to generate a set of algebraic and differential equations or a mathematical model. In order to perform rapid product optimisation iterations, the models must be formulated and evaluated in the most efficient way. Automated environments contribute to this. One of the pioneers of simulation technology in medicine defines simulation as a technique, not a technology, that replaces real experiences with guided experiences reproducing important aspects of the real world in a fully interactive fashion [iii]. In the following chapters the reader will be introduced to the world of simulation in topics of current interest such as medicine, military purposes and their use in industry for diverse applications that range from the use of networks to combining thermal, chemical or electrical aspects, among others. We hope that after reading the different sections of this book we will have succeeded in bringing across what the scientific community is doing in the field of simulation and that it will be to your interest and liking. Lastly, we would like to thank all the authors for their excellent contributions in the different areas of simulation.

INTECH
open science | open minds

InTech Europe
University Campus STeP Ri

InTech China
Unit 405, Office Block, Hotel Equatorial Shanghai

Slavka Krautzeka 83/A
51000 Rijeka, Croatia
Phone: +385 (51) 770 447
Fax: +385 (51) 686 166
www.intechopen.com

No.65, Yan An Road (West), Shanghai, 200040, China
中国上海市延安西路65号上海国际贵都大饭店办公楼405单元
Phone: +86-21-62489820
Fax: +86-21-62489821